The Self-Coherent Camera: a new tool for planet detection

P. Baudoz, A. Boccaletti, J. Baudrand, and D. Rouan

LESIA, Observatoire de Paris-Meudon, France
email: pierre.baudoz@obspm.fr

Abstract. The performance of high contrast imaging systems is very often limited by the presence of static speckles in the point-spread function of the central source. Several techniques have already been proposed to discriminate a faint companion from these residual speckles. These techniques used different criteria to separate a speckle from a companion: polarization, spectral information or coherence. Here, we propose a new imaging device, the Self-Coherent Camera (SCC), that is based on the lack of coherence between the stellar light and the planet that is searched for. This SCC is a simple instrument that allows us to reach the fundamental limitation of the photon noise by calibrating the speckles in the recorded images. After the description of the general problem of discriminating speckles from planets, we will explain the principle of the SCC. Then, we will analyze the different limitations of this technique as well as the performance that can be reached with current telescopes.

Keywords. speckles, coherence.

1. Introduction

Direct imaging of exoplanets requires extremely high dynamical range, high spatial resolution and high sensitivity simultaneously. Different imaging techniques have been proposed to reach such a challenging goal. For example, coronagraphs (Rouan *et al.* 2000), apodized (Soummer *et al.* 2003) or shaped pupil (Kasdin *et al.* 2003) could help reaching the high dynamical range mandatory for direct imaging of exoplanets. However, an essential limitation of these systems is the presence of speckles in the Point Spread Function (PSF). Indeed, while Adaptive Optics (AO) improve greatly the quality of the wavefront of ground based image, there are still residual fast speckles in AO images. These residual atmospheric effects should be averaged quickly with time but, because of defects introduced in the optical system, speckles are still detected on images recorded on ground-based instruments. Slow drifts of the phase errors of optical elements make it difficult to calibrate these speckles that are not fully static. The same kind of drift occurs for space-based telescope where the same kind of speckles are observed. Thus, when attempting to detect a faint companion on long exposure images, one finds that "quasi-static" speckles can be a dominant source of error (Marois *et al.* 2005). The best way to overcome this difficulty is to calibrate these "quasi-static" speckles. Since they are slowly drifting, it is mandatory to find a way to discriminate the speckles of the star from a faint companion during the exposure. This is the purpose of differential imaging techniques. Several criteria have been proposed so far to discriminate the speckles from the planets: spectrophotometry (Racine *et al.* 1999, Marois *et al.* 2005), polarimetry (Seager *et al.* 2000, Baba & Murakami 2003), and coherence (Codona & Angel 2004, Guyon 2004, Labeyrie 2004). While both concepts based on spectrophotometry and polarimetry depends on the physical properties of the planets, the coherence is a robust criterion when no physical information is available from the planets that could be observed. The

techniques based on coherence split the beam in two parts, one used as a coherent reference for the other. The beams are recombined on the same optical axis as in a Michelson interferometer. The recorded interferences are used to control the phase errors with a deformable mirror in Codona & Angel (2004) or an active hologram in Labeyrie (2004) or to calibrate the speckles using a modulated optical path difference (OPD) in Guyon (2004). Here, we suggest another way to calibrate the speckles using coherence as a criterion. The technique we propose rely on a simple Fizeau recombination of the science beam and the reference beam. It enables to discriminate speckles from a planet without using fast OPD modulation or deformable mirrors. After presenting the proposed concept and a possible implementation, we estimate the signal to noise ratio reachable with this technique and show simulations of observations with SCC on a 8 meter telescope.

2. The Self-Coherent Camera concept

The concept of the Self-Coherent Camera (SCC) is described in figure 1 (left). We propose to split the light coming from the telescope into two beams. One of the beam is spatially filtered using a pinhole or an optical fiber. The two beams are recombined in the focal plane in a Fizeau scheme. To do so, the two pupil beams are optically brought at the same plane right before a focusing lens. The distance between the fully coherent pupil and the corrugated pupil is large enough so that their autocorrelation are never superimposing. A possible set-up is shown in figure 1 (right).
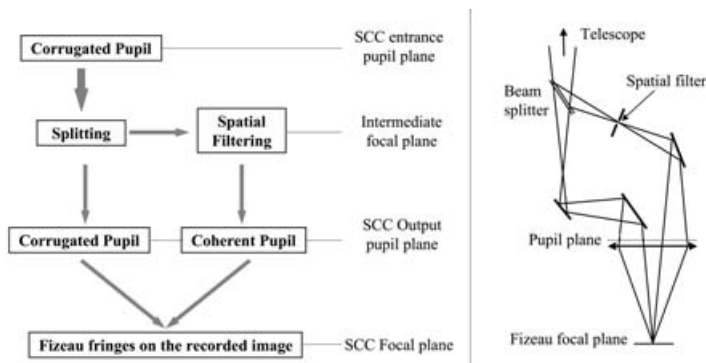

Figure 1. Left: Principle of the Self-Coherent Camera. Right: Possible set-up for the SCC.

The Fizeau image in the focal plane will show fringes pinning the intensity distribution of the stellar flux. Since the flux of the companion is fully removed from the reference beam by spatial filtering, the intensity of the companion will be unaltered by the reference beam. This is what can be seen in figure 2 where the point spread function of the stellar flux interfere with the reference beam creating a fringe pattern over all the diffraction rings and speckles. A companion located at a distance of 2 λ/D and in the upper right quadrant does not show fringes because it is not coherent with the reference beam.

3. Formalism

Assuming the electromagnetic field in the entrance pupil plane is described by $\Psi(\boldsymbol{\xi}) = \widehat{\sqrt{I(\boldsymbol{x})}}$ with $\sqrt{I(\boldsymbol{x})}$ describing the complex amplitude in the focal plane, we can write the field of both the star A and its companion B in the pupil plane:

$$\Psi_A(\boldsymbol{\xi}) + \Psi_B(\boldsymbol{\xi}) = \widehat{\sqrt{I_A(\boldsymbol{x})}} + \widehat{\sqrt{I_B(\boldsymbol{x})}}$$

The coherent pupil of the reference beam can be described in the pupil plane by:

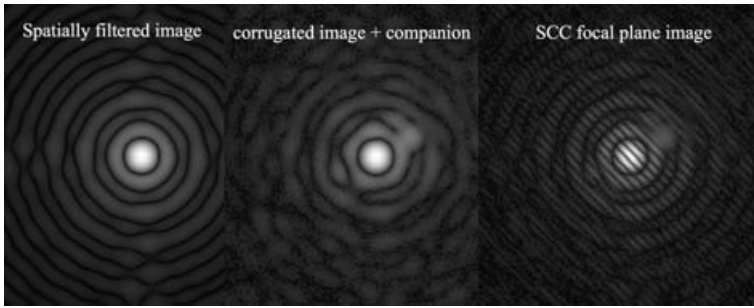$$\Psi_R(\boldsymbol{\xi}) = \widehat{\sqrt{I_R(\boldsymbol{x})}}$$

Figure 2. Left: reference beam. Middle: corrugated beam with a main star and a companion located at a distance of 2 λ/D and in the upper right quadrant. Right: SCC final image plane where the companion does not show Fizeau fringes. The companion is only 20 times fainter that the star. The simulation hypothesis are the same than the one of figure 5.
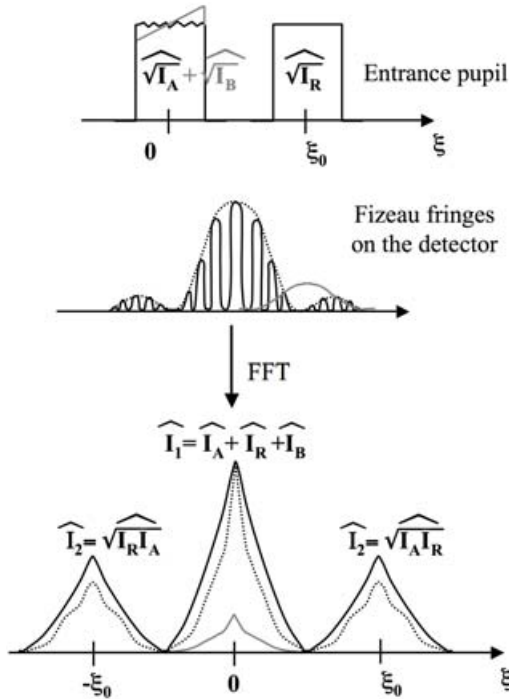

Figure 3. Principle of the SCC. Top: Electromagnetic field distribution in the SCC output pupil plane for a corrugated star (black) and its companion (grey). Middle: Fizeau fringes recorded on the detector for both objects. Bottom: Numerical Fourier Transform of the detected images showing autocorrelations and intercorrelations between the reference beam and the stellar beam.

Assuming that the vector $\boldsymbol{\xi}_0$ describes the distance between the coherent pupil and the corrugated pupil (supposed to be centred on zero). The field at the SCC pupil output plane is given by:

$$\Psi(\boldsymbol{\xi}) = \Psi_A(\boldsymbol{\xi}) + \Psi_B(\boldsymbol{\xi}) + \Psi_R(\boldsymbol{\xi}) * \delta(\boldsymbol{\xi} - \boldsymbol{\xi}_0) \tag{3.1}$$

where $*$ is the convolution symbol. The image recorded at the focal plane following this pupil plane is:

$$I(\boldsymbol{x}) = |\widehat{\Psi(\boldsymbol{\xi})}|^2 = I_A(\boldsymbol{x}) + I_B(\boldsymbol{x}) + I_R(\boldsymbol{x}) +$$

$$2\sqrt{I_A(\boldsymbol{x})I_R(\boldsymbol{x})} \cdot \cos(2\pi\boldsymbol{x}\boldsymbol{\xi}_0) \tag{3.2}$$

Equation 3.2 assumes that there is no optical path difference between both pupils when recombined. If an optical path difference is introduced, it will introduce a phase in the cosinus. Following equation 3.2, the image will look like a classical Fizeau image with fringes pinning the intensity distribution of the main star. However, the image of the companion does not show any fringes because it is not coherent with the reference beam. Since the intensity of the main star is coded with fringes while the image of the companion is not, it looks clearly that one can discriminate the image of the companion from the stellar flux. A good approach is to use the numerical FFT of the image to separate the three areas limited by the autocorrelation of the pupil function. The centred area where appears the autocorrelation of the two different image of the pupil and two lateral terms where appears the correlation between the fields Ψ_A and Ψ_R (Fig. 3). The separation between the two image of the pupil $\boldsymbol{\xi}_0$ is large enough so that the different terms are not superimposed and can be numerically separated.

Assuming that we describe the centred area by $\widehat{I_1(\boldsymbol{x})} = \widehat{I_A(\boldsymbol{x})} + \widehat{I_B(\boldsymbol{x})} + \widehat{I_R(\boldsymbol{x})}$ and the two other area by $\widehat{I_2(\boldsymbol{x})} = \sqrt{\widehat{I_A(\boldsymbol{x})I_R(\boldsymbol{x})}}$, we can write the intensity of the companion using the following formula:

$$I_B(\boldsymbol{x}) = I_1(\boldsymbol{x}) - I_R(\boldsymbol{x}) - \frac{I_2(\boldsymbol{x})^2}{I_R(\boldsymbol{x})} \tag{3.3}$$

To detect the companion $I_B(\boldsymbol{x})$, one needs to record separately $I_R(\boldsymbol{x})$. It can be done because $I_R(\boldsymbol{x})$ is a spatially filtered beam that can be very stable over time.

This equation is valid for an exposure shorter than the coherent time of the atmospheric speckles. Indeed for a long exposure (N times longer than the coherent time), the intensity I_1 and I_2 can be written:

$$I_1(\boldsymbol{x}) = \sum_{i=0}^{N}[I_A^i(\boldsymbol{x}) + I_B^i(\boldsymbol{x})] + N.I_R(\boldsymbol{x})$$

and

$$I_2(\boldsymbol{x}) = I_R(\boldsymbol{x}) \sum_{i=0}^{N}[\sqrt{I_A^i(\boldsymbol{x})}]$$

where $I_A^i(\boldsymbol{x})$ and $I_A^i(\boldsymbol{x})$ varies with atmospheric turbulence (corrected or not).

Obviously equation 3.3 is not any more valid for long exposure because

$$\sum_{i=0}^{N} I_A^i(\boldsymbol{x}) \neq \left[\sum_{i=0}^{N} \sqrt{I_A^i(\boldsymbol{x})}\right]^2$$

For the same reason, equation 3.3 can only be applied to monochromatic beam. However, if observing on small angular distances where the SCC is the most efficient, the bandwidth can be increased up to a reasonable value (R=10). Another way to avoid this issue is to use a chromatic corrector as proposed by Wynne (1979).

The division that appears in equation 3.3 could also be an issue because it increase the noise in the low photon area of $I_R(\boldsymbol{x})$. However, the exposure time for I_R can be much larger than the coherent time because it is a stable beam. So the division will increase the noise at the dark ring positions but can be reduced using a statistical analysis of the recorded images.

4. Simulation

To evaluate the capabilities of the SCC, we first simulated the instrument for a perfect PSF and compared it with direct imaging photon noise. Since the SCC can only record short exposure times, the number of photon per image will be limited and an estimation
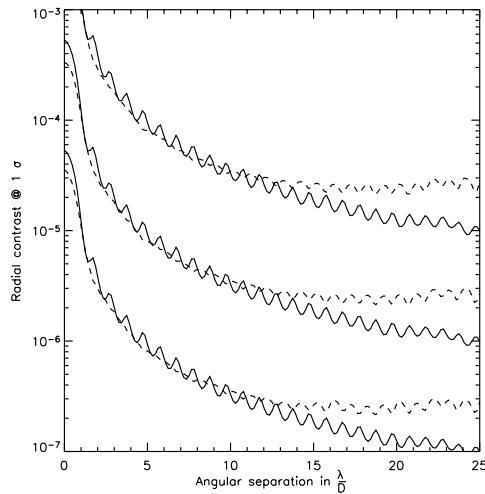
Figure 4. Averaged radial contrast at $1\,\sigma$ with direct imaging (solid) and using SCC (dashed) for 1,100 ,10000 images. Hypothesis: Perfect PSF, $m_H = 5$, $\Phi_{tel} = 8m$, $\lambda_0 = 1.6\mu m$, $\Delta\lambda = 0.3\mu m$, exp. time = 5 ms, total transmission= 0.2. Chromaticity of the PSF is not simulated. RON=0.

of the photon noise effect is needed. To take into account the photon noise, we assumed a star with a magnitude $m_H = 5$ ($\lambda_0 = 1.6\mu m$, $\Delta\lambda = 0.3\mu m$) observed with an 8m-telescope (total transmission of 0.2). The exposure time is set to 5 ms which corresponds roughly to the coherent time in the H band. The Readout Noise (RON) is equal to zero. No chromaticity of the PSF is simulated for this example. The reference beam $I_R(\boldsymbol{x})$ is recorded separately in a single exposure with exposure time of 5 ms , 0.5s and 50s respectively for the 1, 100, 10000 simulated SCC images. This obviously helps decreasing the photon noise introduced by $I_R(\boldsymbol{x})$ in the equation 3.3 for long exposure. Figure 4 shows the averaged radial contrast at $1\,\sigma$ for the SCC and for direct imaging photon noise. Both observation techniques give the same limiting contrast up to 13 λ/D where the SCC techniques hits its limits because the average photon level per pixel becomes lower than one on a single image.

As described in the introduction, the limiting noise when dealing with real AO images is not the photon noise, neither the atmospheric speckle noise that is averaged very quickly but the slow drift of "quasi-static" speckles. To show that the SCC is independent of this noise, we simulated AO images with the same observed star than above introducing phase defects in the wavefronts. The reference beam shows a 10 nm rms typical optical defects (spatial frequency in f^{-2}) and 10000 AO-corrected wavefronts have been simulated. These wavefronts are simulated from an analytical expression of the power spectral density (PSD). This PSD approximates the low frequency by a law in f^{-2} up to the corrected spatial frequency. The level of this part of the PSD is arbitrary chosen to reach a realistic Strehl ratio of about 0.8 in H band. The frequencies above this limit are classical atmospheric law with an outer scale of 20m and a Fried parameter $r_0 = 25cm$. The AO system is supposed to correct 40 by 40 subapertures in the pupil. A Strehl ratio of 0.8 corresponds to a phase aberration of 120 nm rms in the pupil. We add to all the simulated wavefront a fixed phase aberration with the same PSD but 12 times less aberrated (10 nm). As above, the reference beam is recorded separately in a single exposure corresponding to the number of simulated wavefront used when resolving equation 3.3. An example of the reference image, the corrugated image, and the interference between both of them is shown in Figure 2. In Figure 5, the averaged radial contrast at $1\,\sigma$ of the SCC is compared to the theoretical photon noise and to the "quasi-static"
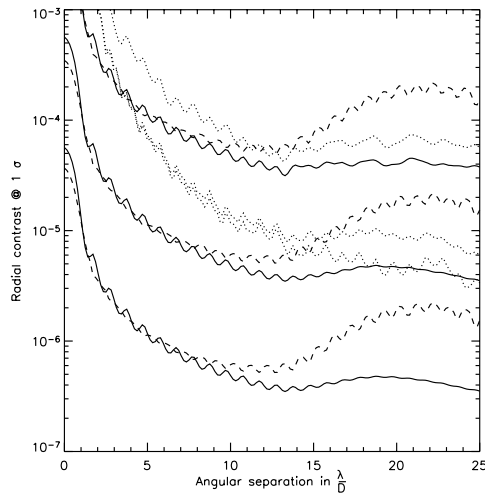
Figure 5. Averaged radial contrast at $1\,\sigma$ for direct imaging with fixed wavefront errors (dotted), for SCC imaging(dashed) and for theoretical photon noise (solid). The simulations for 1,100, and 10000 images are shown. Photon noise with direct imaging and using SCC. Corrugated PSF. Hypothesis: $r_0 = 25cm$, AO $=40\text{x}40$, $Sr = 0.8$ in H band, $m_H = 5$, $\Phi_{tel} = 8m$, $\lambda_0 = 1.6\mu m$, $\Delta\lambda = 0.3\mu m$, exp. time = 5 ms, total transmission= 0.2. Chromaticity of the PSF is not simulated. RON=0. Fixed wavefront error =10nm, Reference beam wavefront error= 10nm.

speckle noise. The SCC is again limited only by the photon noise up to 13 λ/D for the same reason than above. For the "quasi-static" speckle noise, the contrast is limited by the fixed speckle level. The level being 12 times lower than the AO residual aberration, integrating more than 150 images does not improve the contrast.

5. Conclusion

We described a new imaging device that relies on coherence to differentiate a speckle from a true companion. This Self-Coherent Camera (SCC) uses Fizeau fringes in the focal plane to encode the speckles of the star. A simple image processing technique is used to compute from each recorded image the signal of a true companion which is not encoded by fringes. Simulation of a perfect case showed that the photon noise limit can be reached if the flux per pixel is larger than one photon. The SCC is then especially efficient for small angular separation. A more realistic simulation showed that at these small angular separation, the SCC improves the contrast that can be detected even if the images are limited by slowly drifting speckles, which is the case for real AO images.

References

Baba, N. & Murakami, N. 2003, 115, 1363
Codona, J. & Angel, R. 2004, ApJ, 604, L117
Guyon, O. 2004, ApJ, 615, 562
Kasdin, N. J., Vanderbei, R. J., Spergel, D. N., & Littman, M. G. 2003, ApJ, 582, 1147
Labeyrie, A. 2004, Proc. "Astronomy with High Contrast Imaging II", EAS Pub. Series, 12, 3
Marois, C., Doyon, R., Nadeau, D., Racine, R., Riopel, M. Vallée. P., & Lafrenière, D. 2005, PASP, 117, 745
Racine, R., Walker, G., Nadeau, D., Doyon, R., & Marois, C. 1999, PASP, 111, 587
Rouan, D., Riaud, P., Boccaletti, A., Clénet, Y., & Labeyrie, A. 2000, PASP 112, 1479
Seager, S., Whitney, B., & Sasselov, S. 2000, ApJ, 540, 504
Soummer, R., Aime, C., & Falloon, P. E. 2003, A&A, 403, 369
Wynne C. 1979, Opt. Comm., 28, 21